Journal of Solid State Chemistry 181 (2008) 1970–1976

Contents lists available at ScienceDirect

Journal of Solid State Chemistry

journal homepage: www.elsevier.com/locate/jssc

Structural and magnetic properties of $Zn_{1-x}Sb_xCr_{2-x/3}Se_4$ ($x = 0.11$, 0.16 and 0.20) single crystals

E. Malicka [a,*], A. Waśkowska [b], J. Heimann [c], T. Mydlarz [d], R. Sitko [a], D. Kaczorowski [b]

[a] Chemistry Department, University of Silesia, Szkolna 9, 40-006 Katowice, Poland
[b] Institute of Low Temperature and Structure Research, Polish Academy of Sciences, P.O. Box 1410, 50-950 Wrocław, Poland
[c] Institute of Physics, University of Silesia, Uniwersytecka 4, 40-007 Katowice, Poland
[d] International Laboratory of High Magnetic Fields and Low Temperatures, Gajowicka 95, 53-529 Wrocław, Poland

ARTICLE INFO

Article history:
Received 30 December 2007
Received in revised form
30 March 2008
Accepted 16 April 2008
Available online 3 May 2008

Keywords:
Magnetically ordered materials
Single crystals growth
X-ray diffraction
X-ray photoelectron spectroscopy
Magnetic measurements

ABSTRACT

Single crystals of $Zn_{1-x}Sb_xCr_{2-x/3}Se_4$ based on the $ZnCr_2Se_4$ spinel, which is known to exhibit interesting magnetic and electronic transport properties, have been prepared by solid state reaction from the appropriate selenides. Three compounds of different Sb content ($x = 0.11$, 0.16, and 0.20) were studied by X-ray diffraction, X-ray photoelectron scattering technique and macroscopic magnetic measurements with the aim to determine (i) stability of the cubic symmetry and (ii) influence of the Sb admixture on the magnetic properties. The results show that the Sb^{3+} and Zn^{2+} ions share the tetrahedral sites in the spinel structure, while the Cr^{3+}ions carrying magnetic moments, are located in the octahedral sites. The X-ray photoelectron spectroscopy (XPS) data indicate that in this series of compounds the chromium ions have a $3d^3$ electronic configuration. The three samples studied order antiferromagnetically at low temperatures, with the magnetic characteristics being hardly altered with respect to those reported for the parent $ZnCr_2Se_4$ compound.

1. Introduction

$ZnCr_2Se_4$ is a cubic spinel that exhibits interesting structural, magnetic and electronic transport properties, directly related to the presence of localized $3d$ electrons of the Cr^{3+} ions. Below $T_N = 20$ K the compound reveals complex helimagnetic spin order, which results from competing ferromagnetic (F) and antiferromagnetic (AF) interactions [1–13]. Sharp specific heat anomaly, negative thermal expansion, and colossal magnetostriction, altogether pointed out to distinct spin-lattice correlations and spin-driven origin of the tetragonal structure distortion observed below T_N [8]. It was also established that the magnetic order can be fully suppressed by external magnetic field of ~70 kOe, suggesting a field induced quantum-critical behaviour [8,9]. In the paramagnetic region the magnetic behaviour of $ZnCr_2Se_4$ is characterized by the effective magnetic moment $\mu_{eff} = 3.87\,\mu_B$ and the paramagnetic Curie temperature $\theta_p = 115$ K [12,13]. The compound exhibits semiconducting properties with p-type conductivity [6,14].

Much research work was carried out on various diluted spinel systems. In a number of papers it has been shown that replacement of di- or trivalent cations by other metals results in essential changes in the physical properties, where effects of site disorder, lattice frustration and random distribution of spin interactions can be observed [4,5,15]. The influence of trivalent diamagnetic In, Ga and Al admixtures was reported in Refs. [16–22]. Upon incorporating indium atoms into the unit cell of $ZnCr_2Se_4$, the Néel temperature decreases down to 16 K, determined for the maximum In content $x = 0.14$. At the same time, value of the effective magnetic moments gets enhanced, suggesting that in the octahedral B-sites, besides of Cr^{3+} ions with the electronic configuration $3d^3$, also some Cr^{2+} ions with the $3d^4$ configuration may be present [16,17]. The electrical transport studies located this compound among semiconductors with small conductivity values of the order of $10^{-4}\,\Omega^{-1}\,m^{-1}$, which exhibit thermally induced transition from n- to p-type conductivity.

In the solid solutions with Ga^{3+} admixtures, the maximum gallium concentration is $x = 0.4$ [18,19]. The Ga^{3+} ions are accommodated in both the A and B-sites of the spinel structure. With increasing Ga^{3+} content the paramagnetic Curie temperature and the saturation magnetization decrease, while T_N remains unchanged. The compounds are p-type semiconductors, and higher Ga concentration at the B-sites combines with higher values of the electrical conductivity. For the Ga concentration of about $x = 0.4$ some cationic vacancies are present [20,21].

The dilution range of Al^{3+} appeared to be limited to $x = 0.23$. Although the Al^{3+} ions share the B-sites with chromium, the magnetic characteristics of the substituted system, i.e. T_N and

* Corresponding author.
E-mail address: malicka@us.edu.pl (E. Malicka).

0022-4596/$ - see front matter © 2008 Elsevier Inc. All rights reserved.
doi:10.1016/j.jssc.2008.04.022

θ_{C-W}, are very similar to those of the parent compound $ZnCr_2Se_4$. However, with rising x, a rapid reduction in the magnitude of the saturation magnetic moment takes place, hence suggesting systematic changes in the interplay between AF and F interactions due to rising level of lattice disorder and dilution of the magnetic sublattice of Cr^{3+} [22].

The purpose of the present study was to investigate the influence of Sb^{3+} admixture on the stability of the cubic symmetry and on the magnetic properties of $ZnCr_2Se_4$-based spinels. This is continuation of the work series concerning the mechanism of incorporation of three-valent cations into the chromium selenide spinels, and the role of these cations in modifying the magnetic and transport properties. Three single-crystalline samples $Zn_{1-x}Sb_xCr_{2-x/3}Se_4$ with different antimony concentration, grown by chemical vapour transport method, were studied with respect to valence states of cations and their distribution between the tetrahedral and octahedral sites in the spinel lattice. Moreover, the electronic structure of the chromium ions was verified by X-ray photoelectron spectroscopy. The magnetic properties of the system were investigated by means of magnetization and magnetic susceptibility measurements carried out in wide ranges of temperature and magnetic field strength.

2. Experimental

2.1. Synthesis

The single crystal of $Zn_{1-x}Sb_xCr_{2-x/3}Se_4$ samples were grown from the binary selenides ZnSe, Sb_2Se_3 and anhydrous chromium chloride (purity 95%). The latter compound served also as transporting agent in the chemical vapour transport process.

The two binary selenides were synthesized from elemental antimony, zinc and selenium, all with the stated purities better than 99.999%. The stoichiometric mixtures of the elements were pulverized in an agate mortar and sealed in evacuated quartz ampoules. The samples were heated for 7 days at 1073 K, then ground to powder, and heated once more for 7 days at the same temperature as before. The products were checked by X-ray powder diffraction and found to be single-phase materials.

Mixtures of the selenides and $CrCl_3$ were sealed in quartz ampoules (length ~200 mm, inner diameter 20 mm) evacuated to $\sim 10^{-3}$ Pa. Temperature of the crystallization zone was between 1075 and 1179 K, while temperature of the melting zone was in the range 1165–1233 K. The furnace was slowly cooled to room temperature after 3 weeks of heating. The obtained single crystals had regular octahedral shape and well-formed regular (111) faces with edge lengths up to 4 mm.

The presence of antimony in the obtained single crystals was checked by an energy-dispersive X-ray microanalysis (EDAX) with Philips SEM 515 microscope. This helped to select off the samples containing the Sb admixtures. Chemical composition of $Zn_{1-x}Sb_xCr_{2-x/3}Se_4$ was determined by nondestructive energy-dispersive X-ray fluorescence spectrometry (EDXRF). The X-ray spectrum from the sample excited by monochromatic Mo$K\alpha$ radiation was collected by thermoelectrically cooled Si-PIN detector (XR-100CR Amptek, Bedford, MA, USA), having a resolution of 145 eV at 5.9 keV. The pinhole collimator of 1000 μm hole diameter was placed in front of the X-ray detector to reduce size of analysed area of single crystal. The Si-PIN detector was coupled to a multichannel analyser (PX4 Amptek, Bedford, MA, USA). The quantitative EDXRF analysis of single crystal was performed by standardless fundamental parameters method. EDXRF analysis was compared with well-validated wavelength-dispersive X-ray spectrometry (WDXRF) method using sequential spectrometer PW1410 (Philips, Almelo, The Netherlands). For this purpose, some single crystals were analysed by nondestructive EDXRF and then were analysed by WDXRF after their digestion and by using series of multielement calibration samples. The agreement between EDXRF and WDXRF analysis was satisfactory and the relative differences did not exceed 3%. The results of EDXRF analysis together with determined chemical formulae are shown in Table 1.

Table 1
EDXRF analysis for single crystals of $(Zn_{1-x}Sb_x)[Cr_{2-x/3}]Se_4$

Chemical formula	Zn	Sb	Cr	Se
$Zn_{0.89}Sb_{0.11}Cr_{1.97}Se_4$	11.90 ± 0.19	2.71 ± 0.104	20.91 ± 0.25	64.47 ± 0.89
$Zn_{0.84}Sb_{0.16}Cr_{1.95}Se_4$	11.15 ± 0.14	4.02 ± 0.081	20.61 ± 0.32	64.23 ± 1.12
$Zn_{0.80}Sb_{0.20}Cr_{1.92}Se_4$	10.59 ± 0.20	4.97 ± 0.122	20.30 ± 0.29	64.14 ± 0.94

The results are in % (m/m).

2.2. X-ray photoelectron spectroscopy

X-ray photoelectron spectroscopy (XPS) spectra were taken using a PHI 5700/660 Physical Electronic spectrometer with monochromated Al$K\alpha$ radiation. The photoelectron spectra were analysed by a hemispherical mirror analyser with an energy resolution of about 0.3 eV. In order to obtain free of contamination fresh surface, the samples were scraped *in situ* in 10^{-10} hPa vacuum. The following spectra have been measured: (1) an overview of the binding energy in the range −2 to 1400 eV; (2) the valence band in the region −2/20 eV and (3) the core-level characteristic peaks for Se: 3*d*, Cr: 2p, Zn: $2p_{3/2}$, and Sb: 4*d*. The background was subtracted using the Tougaard's approximation.

2.3. X-ray diffraction

Three single crystals of dimensions given in Table 1 and differing in Sb^{3+} content were chosen for X-ray diffraction measurements on a four-circle diffractometer Xcalibur/CCD Oxford Diffraction, operating in κ geometry and using graphite monochromated Mo$K\alpha$ radiation. The intensity data were collected with ω-scan technique and $\Delta\omega$ step of 1.2°. A set of 1080 images taken in nine runs of 120 exposures with different orientations in the reciprocal space, covered almost 99% of the Ewald sphere. The exposure time per one image was 30 s. Crystal and instrument stability were controlled by one image, selected as a standard and measured after each 50 images [23]. The intensity data were integrated and corrected for Lorentz and polarization effects with *CrysAlis* software [24]. Numerical absorption correction based on the crystal shape was applied [24]. The structure refinement was performed using the SHELXL-97 program package [25]. The crystal data and the details of experimental conditions are summarized in Table 2, together with the general results of the structure refinements.

2.4. Magnetic measurements

Magnetization and magnetic susceptibility measurements were performed in the temperature range 1.72–400 K and in magnetic fields up to 5 T employing a Quantum Design MPMS-5 SQUID magnetometer. Moreover, the magnetization was measured at liquid helium temperature in fields up to 14 T using a home-made induction magnetometer. The samples used for magnetic measurements were single crystals of the $Zn_{1-x}Sb_xCr_{2-x/3}Se_4$ compounds, in an amount of about 100 mg, freely placed in a sample holder (drinking straw). Corrections for the sample holder as well as for the core electron diamagnetism were

Table 2
Crystal data, experimental details and structure refinements results for $(Zn_{1-x}Sb_x)[Cr_{2-x/3}]Se_4$ ($x = 0.11$, 0.16 and 0.20)

Crystal data	$(Zn_{0.89}Sb_{0.11})Cr_{1.97}Se_4$	$(Zn_{0.84}Sb_{0.16})Cr_{1.95}Se_4$	$(Zn_{0.80}Sb_{0.20})Cr_{1.92}Se_4$
Crystal system, space group	Cubic, $Fd\bar{3}m$	Cubic, $Fd\bar{3}m$	Cubic, $Fd\bar{3}m$
Unit cell dimensions (Å)			
a	10.498(1)	10.511(1)	10.526(1)
Volume (Å^3)	1156.03(3)	1161.27(3)	1166.25(3)
Z	8	8	8
Calculated density (Mg/m^3)	5.637	5.659	5.687
Crystal size (mm)	$0.07 \times 0.08 \times 0.08$	$0.09 \times 0.09 \times 0.09$	$0.8 \times 0.10 \times 0.10$
Data collection			
Wavelength (Å)	0.71073	0.71073	0.71073
$2\theta_{max}$ for data collection	89.43	92.83	92.65
Limiting indices:			
h	−13, 13	−14, 14	−11, 13
k	−13, 13	−14, 14	−13, 13
l	−12, 13	−14, 9	−13, 13
Reflections collected	4696	5067	4460
Reflections unique	153	182	154
Reflections $>2\sigma(I)$]	146	147	143
Absorption coefficient (mm^{-1})	32.88	32.78	32.69
R(int)	0.042	0.051	0.049
Refinement			
Refinement method	Full-matrix least-squares on F^2		
Number of refined parameters	10	10	10
Goodness-of-fit on F^2	1.012	1.018	1.005
Final R indices [$I>2\sigma(I)$] R_1	0.019	0.022	0.019
wR_2	0.040	0.043	0.038
Extinction coefficient	0.0011(1)	0.0002(1)	0.0030(1)
Largest diff. peak and hole (e Å^{-3})	0.68 and −0.85	1.1 and −0.98	1.02 and −0.84

found to be negligible in comparison with the signal due to the samples in both the ordered and paramagnetic regions.

3. Results and discussion

The magnetic properties of the compounds under study depend mainly on the electronic configuration of Cr^{n+} ions and distribution of the cations between the tetrahedral and octahedral voids of the cubic closed-packed selenium sublattice. Therefore, we focused our attention on precise determination of the cation positions based on a single-crystal X-ray diffraction technique. Besides, the electronic structure of chromium ions was independently studied by XPS, the technique, which can provide valuable information on the local magnetic moments at the 3*d* metals [26].

3.1. Cation distribution

The origin of the unit cell was taken at the point $\bar{3}m$ of the space group $Fd\bar{3}m$ (No. 227). In the normal spinel the Zn^{2+} ions are located at the tetrahedral position 8*a*: $(\frac{1}{8},\frac{1}{8},\frac{1}{8})$ (*A* site), and the Cr^{3+} ions at the position 16*d*: $(\frac{1}{2},\frac{1}{2},\frac{1}{2})$ (*B* site). In the first approach to the structure refinement an attempt was made to refine the Sb and Cr ions sharing the *B* sites with coupled site occupancy factors (SOF) and constrained atomic displacements. Because of strong correlation, the SOFs for Sb and Cr were refined separately in alternative runs of calculations. The convergence resulted in rejection of Sb from the octahedral sites. Similar procedure applied to Sb located in the tetrahedral *A* sites led to the acceptable atomic displacement parameters and SOFs, which allowed writing the chemical composition formula as given in Table 3. On the other hand the somewhat enhanced thermal displacements in the *A* site may indicate a static positional disorder of Zn^{2+}/Sb^{3+} pseudo-ion, which is primarily driven by a difference in the ionic charges as well as in ionic and covalent radii ($r^i_{Zn} = 0.60$, $r^i_{Sb} = 0.76$ and $R^c_{Zn} = 1.33$, $R^c_{Sb} = 1.41$, where upper indices denote the ionic and covalent radii, respectively) [27–29]. Since the radius for Sb^{3+} is the same in the tetrahedral and octahedral coordination, it seems that the governing factor in the cation distribution is very strong octahedral preference of Cr^{3+} [30]. This explains why the *A*-site location for Sb was found in all the samples studied. The Sb concentration did not exceed the critical quantity for isomorphous substitution, preserving the spinel structure. However, the location of the Sb^{3+} ions in the tetrahedral voids implies, for the electrostatic charge compensation, some decrease in the total number of the Cr^{3+} ions in the octahedral sites. Since the XPS study (see below) gives no evidence of the charge disproportionation of chromium, which could lead to an appearance of the Cr^{2+} and Cr^{4+} pairs, the respective number of the Cr^{3+} vacancies should be taken into account. This assumption found confirmation in the results of the SOF refinement for Cr atoms. In all the samples a certain Cr deficit has been observed. Thus, the chemical formula can be written as $(Zn^{2+}_{1-x}Sb^{3+}_x)[Cr^{3+}_{2-x/3}]Se_4$, where $x = 0.11$, 0,16 and 0.20. The Sb presence in $ZnCr_2Se_4$ is combined with a slightly enlarged unit cell volume (Table 2). The Se positional parameter u, which is a measure of the anion sublattice distortion from the cubic-close packing, remains nearly unchanged compared to $u = 0.259$ in the parent phase $ZnCr_2Se_4$ (Table 3). Some other results of the structure refinements are also given in Table 3, while the selected bond distances and angles are presented in Table 4.

3.2. X-ray photoelectron spectra and Cr valence state

The binding energy of the characteristic core peaks of the respective elements is nearly independent of the admixture concentration. The effect observed for different spinel systems has already been discussed in the literature [31]. Moreover, the 2*p* peaks of Zn, are not shifted relative to the elemental zinc along the

Table 3
Atomic coordinates and equivalent isotropic displacement parameters for $(Zn_{1-x}Sb_x)[Cr_{2-x/3}]Se_4$ ($x = 0.11$, 0.16 and 0.20)

Compound	Anion positional parameter:	SOF in (*A*)-site	SOF in [*B*]-site	U_{iso} (Å$^2 \times 10)^3$	U_{eq} (Å$^2 \times 10^3$)	
	u	Zn/Sb	Cr	Zn/Sb	Cr	Se
$(Zn_{0.89}Sb_{0.11})Cr_{1.97}Se_4$	0.25913(2)	0.89(9)/0.11	0.980(10)	15.1(3)	8.6(2)	8.9(1)
$(Zn_{0.84}Sb_{0.16})Cr_{1.95}Se_4$	0.25925(3)	0.84(10)/0.16	0.975(11)	15.8(3)	7.8(2)	8.2(1)
$(Zn_{0.80}Sb_{0.20})Cr_{1.92}Se_4$	0.25936(3)	0.80(8)/0.20	0.967(9)	15.3(3)	7.4(2)	8.1(2)

Note: The atomic positions are as follows:

Zn/Sb	(*A*) site	8*a*	$(\frac{1}{8},\frac{1}{8},\frac{1}{8})$
Cr	[*B*] site	16*d*	$(\frac{1}{2},\frac{1}{2},\frac{1}{2})$
Se	Anion site	32*e*	(u,u,u)

Table 4
Selected interatomic distances (Å) and angles (deg) for $(Zn_{1-x}Sb_x)[Cr_{2-x/3}]Se_4$

	$(Zn_{0.89}Sb_{0.11})Cr_{1.97}Se_4$	$(Zn_{0.84}Sb_{0.16})Cr_{1.95}Se_4$	$(Zn_{0.80}Sb_{0.20})Cr_{1.92}Se_4$
Zn/Sb–Se	2.4436(5) × 4	2.4441(5) × 4	2.4496(5) × 4
Cr–Se	2.5324(4) × 6	2.5343(4) × 6	2.5368(4) × 6
Se–Cr–Se	180.00(1) × 3	180.00(1) × 3	180.00(1) × 3
Se–Cr–Se	94.50(1) × 6	95.48(1) × 6	94.54(1) × 6
Se–Cr–Se	85.50(1) × 6	84.52(1) × 6	85.46(1) × 6
Se–Zn–Se	109.47(0) × 6	109.47(0) × 6	109.47(0) × 6

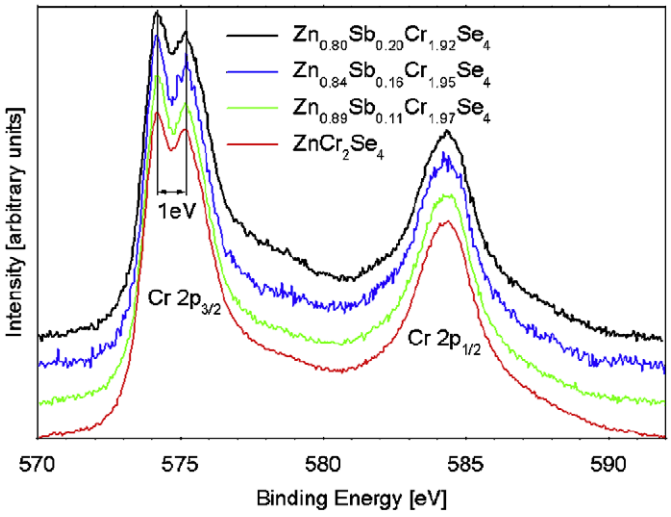

Fig. 1. XPS spectrum of Cr 2*p* core-levels in the $(Zn_{1-x}Sb_x)[Cr_{2-x/3}]Se_4$ system ($x = 0.11$, 0.16 and 0.20).

crystal series. The characteristic Cr 2*p* spectra, which consist of Cr $2p_{3/2}$ and Cr $2p_{1/2}$ peaks are shown in Fig. 1. The Cr $2p_{3/2}$ states are split into two peaks at 574.2 and 575.2 eV. The peak separation with the binding energy difference $\Delta E \approx 1$ eV is typical of the 3*d* elements with localized magnetic moment of 3 μ_B. A similar value of ΔE was reported for $CdCr_2Se_4$ and for a number of other chalcogenide spinels [32]. For Cr_2O_3 the experimental Cr $2p_{3/2}$ splitting was qualitatively described by a strict *ab initio* model [33]. This feature was found also for the manganese $2p_{3/2}$ levels in the Mn^{2+} based spinels [34] and Heusler alloys [35]. It is important to notice that splitting of the $2p_{3/2}$ states can be observed experimentally only for the 3*d* elements with localized magnetic moments larger than 2 μ_B [26,35]. Moreover, a linear relationship has been reported between the magnitude of the splitting of the $2p_{3/2}$ levels and the valence state of the 3*d* transition metals [26]. Based on these findings it can be concluded

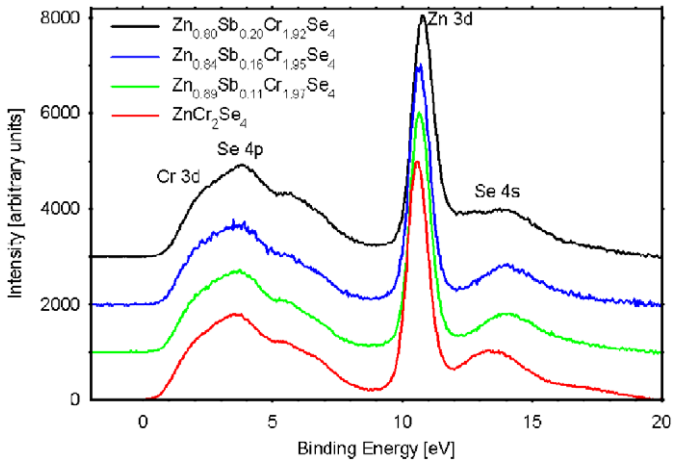

Fig. 2. XPS valence band spectra of the $(Zn_{1-x}Sb_x)[Cr_{2-x/3}]Se_4$ system ($x = 0.11$, 0.16 and 0.20).

that the Cr ions in the $(Zn_{1-x}Sb_x)[Cr_{2-x/3}]Se_4$ system have the electronic state Cr^{3+} $3d^3$.

The XPS valence band spectra of the $(Zn_{1-x}Sb_x)[Cr_{2-x/3}]Se_4$ spinels are shown in Fig. 2. The dominant feature in the region from −2 to 20 eV is a 3*d* Zn peak. Apparently, the substitution of Zn by antimony causes a decrease of the peak area, compared to $ZnCr_2Se_4$, and a shift of the Zn 3*d* states away from the Fermi level. Similar shift of the Se 4*s* states is probably connected with hybridization of these states with the Zn 3*d* states. With increasing Sb content the Se 4*s* band gradually flattens. Near the Fermi level the valence bands of the $(Zn_{1-x}Sb_x)[Cr_{2-x/3}]Se_4$ consist mainly of the Cr 3*d* and Se 4*p* levels. In this region no visible difference, related to the presence of Sb admixture, can be observed because the selenium and chromium sublattices remain nearly unaffected along the series.

3.3. Magnetic properties

The magnetic characteristics of the $(Zn_{1-x}Sb_x)[Cr_{2-x/3}]Se_4$ system are summarized in Figs. 3 and 4. In general, the observed behaviour is very similar to that reported in the literature for the parent compound $ZnCr_2Se_4$ [1–13]. In each case the magnetic susceptibility follows a Curie-Weiss law only above room temperature with the effective magnetic moment of about 3.8 μ_B (Table 5), which is close to the spin-only value for free Cr^{3+} ion with $3d^3$ configuration (3.86 μ_B), seen also for $ZnCr_2Se_4$ [11,12]. The paramagnetic Curie temperature gradually decreases with rising Sb-content from 115 K reported for $ZnCr_2Se_4$ [11,12] to about 108 K in $(Zn_{0.89}Sb_{0.11})Cr_{1.97}Se_4$, 106 K in $(Zn_{0.84}Sb_{0.16})Cr_{1.95}Se_4$, and

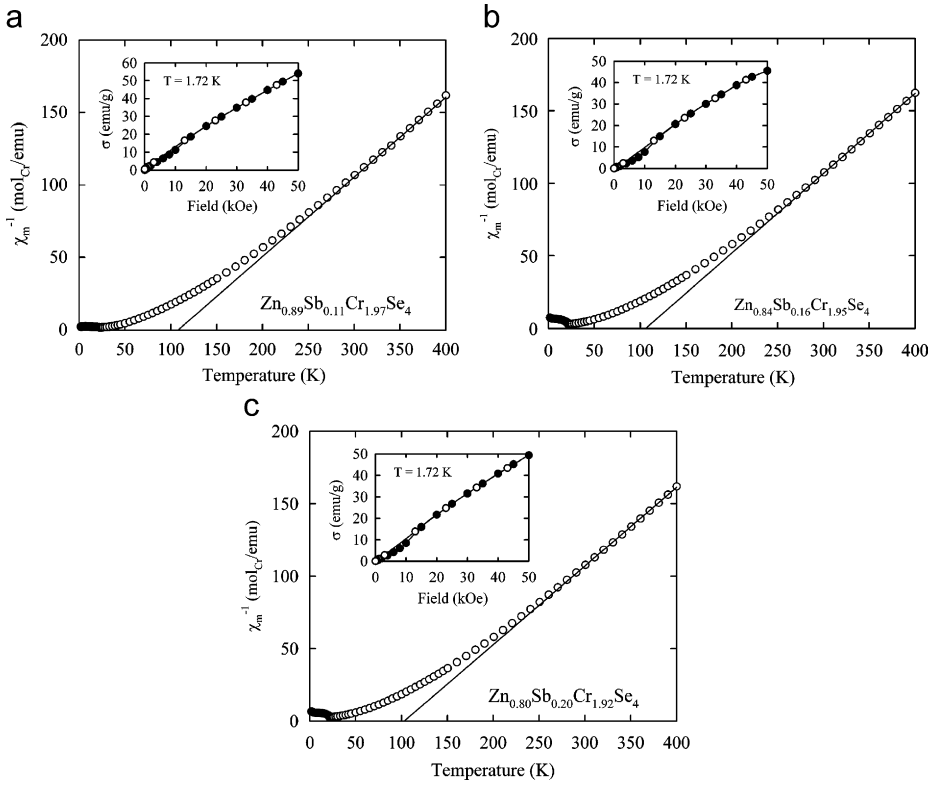

Fig. 3. Temperature dependencies of the inverse molar magnetic susceptibility measured in a field of 1 kOe for $(Zn_{1-x}Sb_x)[Cr_{2-x/3}]Se_4$ ($x = 0.11$, 0.16 and 0.20). The solid curves emphasize a straight-line behaviour of $\chi^{-1}(T)$ at high temperatures. Insets: magnetic field variations of the magnetization, measured at 1.72 K with increasing (full circles) and decreasing (open circles) magnetic field.

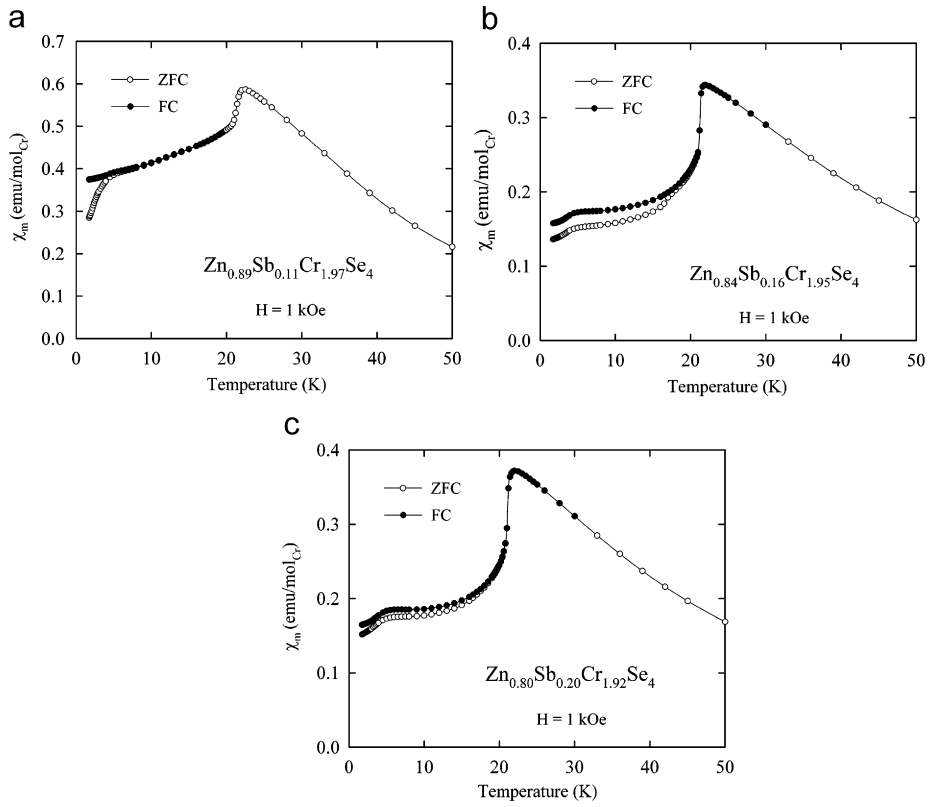

Fig. 4. Low-temperature dependencies of the molar magnetic susceptibility of $(Zn_{1-x}Sb_x)[Cr_{2-x/3}]Se_4$ ($x = 0.11$, 0.16 and 0.20) measured in a field of 1 kOe upon cooling the specimens in zero (ZFC, open circles) and applied (FC, full circles) magnetic field.

Table 5
Magnetic characteristics of the $(Zn_{1-x}Sb_x)[Cr_{2-x/3}]Se_4$ system

x	T_N (K)	θ_p (K)	μ_{eff} (μ_B/Cr atom)	$\mu_{1.7\,K,50\,kOe}$ (μ_B/Cr atom)	μ_{sat} (μ_B/Cr atom)
0.0	20 [11–13] 22 [18]	115 [11,12]	3.87 [11,12]	2.4 [8]	2.98 [18]
0.11	22.0(4)	108(1)	3.81(2)	2.41(2)	2.90(2)
0.16	21.7(2)	106(1)	3.81(3)	2.06(3)	2.83(2)
0.20	21.8(3)	103(1)	3.84(2)	2.26(2)	2.64(3)

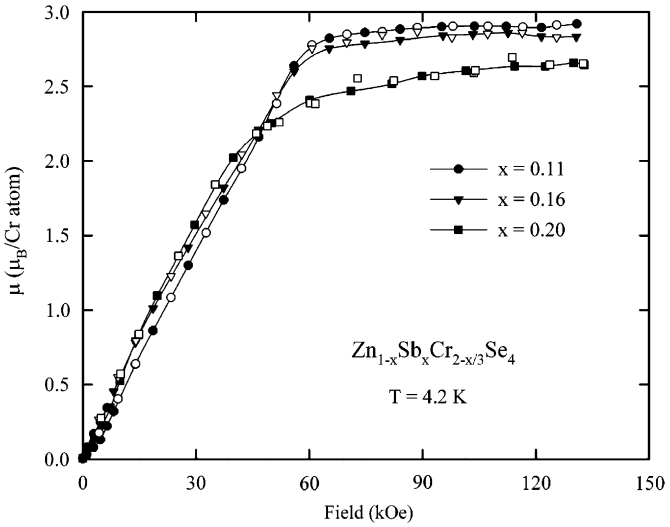

Fig. 5. Magnetic field variations of the chromium magnetic moment in $(Zn_{1-x}Sb_x)[Cr_{2-x/3}]Se_4$ ($x = 0.11$, 0.16 and 0.20).

finally to 103 K in $(Zn_{0.80}Sb_{0.20})Cr_{1.92}Se_4$. The observed trend may signal some changes in the competition between ferromagnetic and antiferromagnetic exchange interactions. In the paramagnetic region below 300 K the $\chi^{-1}(T)$ curves distinctly deviate from a straight-line behaviour, probably due to strong contribution of spin fluctuations. For all three compositions the Néel temperature amounts to about 22 K being equal to that of pure $ZnCr_2Se_4$ [18] (a lower value of 20 K was reported in Refs. [11,12]), as well as to the T_N value derived recently for $Zn[Cr_{1.85}Al_{0.15}]Se_4$ and $Zn[Cr_{1.77}Al_{0.23}]Se_4$ [22].

As it is seen in Fig. 4, the magnetic phase transition is very sharp, characteristic of first-order-type transitions, and very similar in character to that of the parent spinel [1–13,18]. Some irreversibilities in the susceptibility measured upon cooling the specimens in zero and nonzero applied magnetic field are also reminiscent of the behaviour of $ZnCr_2Se_4$ (see for example most recent study reported in Ref. [8]). This effect may be due to the presence of ferromagnetic components in the nominally antiferromagnetic (helimagnetic) structure. Another possibility is the formation below T_N of a spin-glass-like state, which is very likely to occur in geometrically frustrated magnets.

Shown in the insets in Fig. 3 are the magnetic field dependencies of the magnetization in the $(Zn_{1-x}Sb_x)[Cr_{2-x/3}]Se_4$ compounds, measured much below T_N. Changes in the slope of the $\sigma(H)$ curves taken with increasing field, which occur near 10 kOe for all three compositions, can be identified with the metamagnetic-like phase transition observed for the parent spinel [8]. Up to 50 kOe the magnetization is slightly curvilinear function of the applied field strength with no tendency to saturate (the values of the magnetic moment measured at 1.72 K in a field of 50 kOe are given in Table 5). However, as presented in Fig. 5, the saturation is observed in higher fields, actually above the second metamagnetic critical field of about 60 kOe that probably manifests breakdown of the helical spin structure. On rising the concentration of Sb atoms the saturation magnetic moment continuously decreases from $\mu_{sat} = 2.98\,\mu_B$/Cr atom reported for $ZnCr_2Se_4$ [18] to 2.64 μ_B/Cr atom found for $(Zn_{0.80}Sb_{0.20})[Cr_{1.92}]Se_4$ (see Table 5). This feature may be related to the changes in the interplay between the antiferromagnetic and ferromagnetic exchange interactions caused by Zn/Sb substitution and possibly by a presence of some Cr vacancies in the octahedral sites.

4. Conclusions

The dilution range of Sb^{3+} in $ZnCr_2Se_4$ does not exceed the critical concentration for isomorphous substitution preserving cubic spinel structure, and good quality crystals have been obtained for the admixture concentration of $x \leqslant 0.20$. The X-ray diffraction results show that the Sb^{3+} ions share the tetrahedral positions with the Zn^{2+} ions, causing slight increase of the unit cell volume. The observed small deviations of the anionic positional parameter u from the ideal value of 0.250 signal some distortions of the selenium sublattice. The X-ray photoelectron spectroscopy data indicate the $3d^3$ electronic configuration of Cr^{3+} ion with localized magnetic moment of about 3 μ_B. This finding is fully consistent with the results of bulk magnetic measurements. The antiferromagnetic behaviour of the $(Zn_{1-x}Sb_x)[Cr_{2-x/3}]Se_4$ system is very similar to that of the parent spinel $ZnCr_2Se_4$. With increasing Sb-content, some changes in the strength of competing antiferromagnetic and ferromagnetic exchange interactions likely occur, which are manifested via the systematic decrease in the values of the saturation magnetic moment per Cr atom and the paramagnetic Curie temperature. The other magnetic characteristics like the critical metamagnetic fields, the ordering temperatures, the effective magnetic moments and extent of strong spin fluctuations in the paramagnetic state are nearly the same as in $ZnCr_2Se_4$.

Acknowledgment

This study was supported by the Grant 1784/B/H03/2007/33 from the Ministry of Science and Higher Education in Poland.

References

[1] P.K. Baltzer, H.W. Lehman, M. Robbins, Phys. Rev. Let. 15 (1965) 493–495.
[2] V.Y. Kalinnikov, T.G. Aminov, V.M. Novotortsev, Neorg. Mater. 39 (2003) 997–1012 [Inorg. Mater. (Engl. Trans. 39 (2003) 1159–1176].
[3] G. Güner, F. Yildiz, B. Rameev, B. Atkaç, J. Phys.: Condens. Matter 17 (2005) 3943–3952.
[4] A. Wiedemann, M. Hamedoun, J. Rossat-Mignod, J. Phys. C: Solid State Phys. 18 (1985) 2549–2561.
[5] M. Hamedoun, A. Wiedemann, J.L. Dormann, M. Nogues, J. Rossat-Mignod, J. Phys. C: Solid State Phys. 19 (1986) 1801–1811.
[6] M. Nogues, M. Hamedoun, J.L. Dormann, A. Saifi, J. Magn. Magn. Mater. 54–57 (1986) 85–86.
[7] S.K. Sampath, D.G. Kanhere, R. Pandey, J. Phys.: Condens. Matter 11 (1999) 3635–3644.

[8] J. Hemberger, H.-A. Krug von Nidda, V. Tsurkan, A. Loidl, Phys. Rev. Lett. 98 (2007) 147203–147204.
[9] T. Rudolf, Ch. Kant, F. Mayr, J. Hemberger, V. Tsurkan, A. Loidl, Phys. Rev. B 76 (2007) 174307–174310.
[10] R. Plumier, Compt. Rend. Acad. Sci. (France) 260 (1965) 3348–3350.
[11] F.K. Lotgering, Phillips Res. Rep. 11 (1956), 218 and 337.
[12] P.K. Baltzer, P.J. Wojtowicz, M. Robbins, E. Lopatin, Phys. Rev. 151 (1966) 367–377.
[13] J. Akimitsu, K. Siratori, G. Shirane, M. Iizumi, T. Watanabe, J. Phys. Soc. Japan 44 (1978) 172–180.
[14] T. Watanabe, Phys. Soc. Japan 37 (1974) 140–144.
[15] A.K.M. Zakaria, M.A. Asgar, J. Alloys Compd. 396 (2005) 44–53.
[16] J. Krok-Kowalski, J. Warczewski, T. Mydlarz, A. Pacyna, A. Bombik, J. Kopyczok, I. Okońska-Kozłowska, J. Magn. Magn. Mater. 111 (1992) 50–52.
[17] T. Groń, Phil. Mag. B 70 (1994) 121–132.
[18] S. Juszczyk, J. Krok, I. Okońska-Kozłowska, T. Mydlarz, A. Gilewski, J. Magn. Magn. Mater. 46 (1984) 105–113.
[19] I. Okońska-Kozłowska, E. Malicka, A. Waśkowska, T. Mydlarz, J. Solid State Chem. 148 (1999) 215–219.
[20] T. Groń, H. Duda, J. Warczewski, Phys. Rev. B 41 (1990) 12424–12431.
[21] T. Groń, E. Malicka, I. Okońska-Kozłowska, A. Waśkowska, Ferrites: Proceedings of the Eighth International Conference on Ferrites, Kyoto and Tokyo, 2000, p. 211.
[22] E. Malicka, A. Waśkowska, T. Mydlarz, D. Kaczorowski, J. Alloys Compd. 440 (2007) 1–5.
[23] Oxford Diffraction, CrysAlis CCD. Data Collection software, Oxford Diffraction Ltd., Wrocław, Poland, 2001.
[24] Oxford Diffraction, CrysAlis RED. Data Reduction program. Issue 171.32, Oxford Diffraction Ltd., Wrocław, Poland, 2006.
[25] G.M. Sheldrick, SHELXL-99, Program for Crystal Structure Refinement, University of Göttingen, 1999.
[26] S. Plogmann, T. Schlathölter, J. Braun, M. Neumann, Yu.M. Yarmoshenko, M.V. Yablonskikh, E.I. Shreder, E.Z. Kumarev, A. Wrona, A. Ślebarski, Phys. Rev. B 60 (1999) 6428–6438.
[27] I.D. Brown, Acta Crystallogr. B 48 (1992) 553–572.
[28] R.D. Shanon, Acta Crystallogr. A 32 (1976) 751–767.
[29] A. Weiss, H. Witte, Kristallstruktur und chemische Bindung, Verlag Chemie, Weinheim, 1983.
[30] G.M. Sheldrick, Acta Crystallogr. A 64 (2008) 112–122.
[31] E. Agostinelli, C. Battistoni, D. Fiorani, G. Mattogno, M. Nogues, J. Phys. Chem. Solids 50 (1989) 269–272.
[32] V. Tsurkan, St. Plogmann, M. Demeter, D. Hartmann, M. Neumann, Eur. Phys. J. B 15 (2000) 401–403.
[33] E.S. Ilton, W.A. de Jong, P.S. Bagus, Phys. Rev. B 68 (2003) 125106–125108.
[34] S. Åsbrink, A. Waśkowska, L. Gerward, J. Staun Olsen, E. Talik, Phys. Rev. B 60 (1999) 12651–12656.
[35] A. Ślebarski, M. Neumann, B. Schneider, J. Phys.: Condens. Matter 13 (2001) 5515–5518.